Journal Pre-proofs

High near-room temperature figure of merit of n-type Bi_2GeTe_4-based thermoelectric materials via a stepwise optimization of carrier concentration

Liang-Cao Yin, Wei-Di Liu, Xiao-Lei Shi, Han Gao, Meng Li, De-Zhuang Wang, Hao Wu, Liangzhi Kou, Haizhong Guo, Yifeng Wang, Qingfeng Liu, Zhi-Gang Chen

PII: S1385-8947(21)05349-3
DOI: https://doi.org/10.1016/j.cej.2021.133775
Reference: CEJ 133775

To appear in: *Chemical Engineering Journal*

Received Date: 27 October 2021
Revised Date: 9 November 2021
Accepted Date: 18 November 2021

Please cite this article as: L-C. Yin, W-D. Liu, X-L. Shi, H. Gao, M. Li, D-Z. Wang, H. Wu, L. Kou, H. Guo, Y. Wang, Q. Liu, Z-G. Chen, High near-room temperature figure of merit of n-type Bi_2GeTe_4-based thermoelectric materials via a stepwise optimization of carrier concentration, *Chemical Engineering Journal* (2021), doi: https://doi.org/10.1016/j.cej.2021.133775

This is a PDF file of an article that has undergone enhancements after acceptance, such as the addition of a cover page and metadata, and formatting for readability, but it is not yet the definitive version of record. This version will undergo additional copyediting, typesetting and review before it is published in its final form, but we are providing this version to give early visibility of the article. Please note that, during the production process, errors may be discovered which could affect the content, and all legal disclaimers that apply to the journal pertain.

© 2021 Elsevier B.V. All rights reserved.

High near-room temperature figure of merit of n-type Bi_2GeTe_4-based thermoelectric materials via a stepwise optimization of carrier concentration

Liang-Cao Yin,[#a] Wei-Di Liu,[#b,c] Xiao-Lei Shi,[b, c] Han Gao,[d] Meng Li,[c] De-Zhuang Wang,[a] Hao Wu,[a] Liangzhi Kou,[e] Haizhong Guo,[d] Yifeng Wang,[f] Qingfeng Liu,[a,g,] and Zhi-Gang Chen,[b,h,*]*

[a]State Key Laboratory of Materials-Oriented Chemical Engineering, College of Chemical Engineering, Nanjing Tech University, Nanjing 211816, China.

[b]Centre for Future Materials, University of Southern Queensland, Springfield Central, QLD 4300, Australia.

[c]School of Mechanical and Mining Engineering, the University of Queensland, Brisbane, QLD, 4072, Australia.

[d]Key Laboratory of Material Physics of Ministry of Education, School of Physics and Microelectronics, Zhengzhou University, Zhengzhou 450052, China.

[e]School of Mechanical, Medical & Process Engineering, Queensland University of Technology, Brisbane, QLD 4000, Australia.

[f]College of Materials Science and Engineering, Nanjing Tech University, Nanjing 211816, China.

[g]CAS Key Laboratory of Carbon Materials, Institute of Coal Chemistry, Chinese Academy of Sciences, Taiyuan 030001, China

[h]School of Chemistry and Physics, Queensland University of Technology, Brisbane, Queensland 4000, Australia.

[*]Corresponding author. Email: qfliu@njtech.edu.cn; zhigang.chen@usq.edu.au;

[#]These authors contributed equally to this study.

Keywords: Bi_2GeTe_4, thermoelectric, carrier concentration, optimization, *zT*

Abstract

Bi_2GeTe_4 is a promising near room-temperature thermoelectric candidate with a low lattice thermal conductivity. Carrier concentration of intrinsic Bi_2GeTe_4 changes dramatically with tiny Ge content adjustment, leading to a challenge in carrier concentration optimization. To overcome this challenge, we firstly introduce excessive Ge into Bi_2GeTe_4 to shift the Fermi level deep into the conduction band and transfer Bi_2GeTe_4 into a highly degenerate n-type semiconductor. Secondly, the embedded p-type $Bi_2Ge_2Te_5$ secondary phase induces further optimization of the Fermi level and carrier concentration. Finally, the power factor of the as-synthesized Bi_2GeTe_4-based material is significantly increased from ~0.08 μW cm^{-1} K^{-2} to ~4.2 μW cm^{-1} K^{-2} at 423 K when increasing the nominal Ge content (x) of $Bi_2Ge_xTe_4$ from 1 to 1.45. Correspondingly, a high figure-of-merit of ~0.22 at 423 K is achieved in Bi_2GeTe_4-based thermoelectric materials. This result indicates our viable stepwise strategy can be used to optimize carrier concentration and achieve high thermoelectric performance of the n-type Bi_2GeTe_4.

Journal Pre-proofs

1. Introduction

With the growing demand for eco-friendly and renewable energy resources over the past decades, thermoelectric materials have attracted wide attention.[1-5] Energy conversion efficiency of a thermoelectric material is governed by the dimensionless figure-of-merit (zT), described as $zT=S^2\sigma T/\kappa$, where S, σ, T and κ are the Seebeck coefficient, electrical conductivity, absolute temperature, and total thermal conductivity, respectively.[6-12] $S^2\sigma$ is defined as the power factor to identify the electrical performance.[13,14] κ is the sum of electrical (κ_e) and lattice (κ_l) thermal conductivities.[15,16] Performance engineering strategies, such as carrier concentration (n_c, n_e for n-type semi-conductors and n_h for p-type semi-conductors) optimization,[17,18] modulation doping,[19-23] quantum confinement,[24-27] band degeneracy[28-32] and local distortion of the density of states (DOS),[33-35] can effectively increase $S^2\sigma$ and zT. In addition, the reduction of κ_l via various approaches, such as strengthening the intrinsic phonon-phonon interactions,[36] introducing dense point defects,[37-40] additional nanoprecipitates[41-43] and stacking faults.[44] These strategies can also effectively enhance zT. Basically, excellent thermoelectric materials require relatively low κ_l, such as GeTe (~0.83 W m^{-1} K^{-1} at 773 K)[45], Bi_2Te_3 (~0.7 W m^{-1} K^{-1} at 300 K)[46] and SnSe (~0.5 W m^{-1} K^{-1} at 800 K)[47].

Most recently, the thermoelectric performance of IV-V-VI ternary compounds have aroused intensive interest in thermoelectric community, due to intrinsically low κ_l. Y. Gan, *et al* predict a group of 56 novel layered semiconducting IV–V–VI (IV = Si, Ge Sn, Pb; V = As, Sb, Bi; VI = S, Se, Te) compounds and demonstrate that most of these semiconductors fall below 1 W m^{-1} K^{-1} at room temperature.[48] $PbBi_2S_4$ reveals extremely low κ_l of less than 0.46 W m^{-1} K^{-1} over the entire temperature range and the peak zT of 0.46 is achieved at 800 K.[49] $MnBi_4S_{7-x}Se_{7x}$ solid solution features intrinsically low κ_l of 0.5-0.8 W m^{-1} K^{-1} in the temperature range of 300–800 K and a peak zT of ~0.31 at 770 K is observed in $MnBi_4S_{5.46}Se_{1.4}$.[50] $Pb_7Bi_4Se_{13}$ based lillianites achieve an ultralow κ_l of 0.17 W m^{-1} K^{-1} at 800 K in n-type

$(Pb_{0.95}Ga_{0.05})Bi_4Se_{13}$. Therefore, a high peak zT of 1.35 at 800 K and a decent average zT of 0.92 from 450 to 800 K are achieved in $(Pb_{0.95}Ga_{0.05})Bi_4Se_{13}$.[51]

Bi_2GeTe_4 is a promising near room-temperature IV-V-VI ternary thermoelectric material with a low κ_l of ~0.29 W m^{-1} K^{-1} at ~350 K.[52] The stable phase of Bi_2GeTe_4 has a hexagonal structure (space group *R3m*) with the lattice parameters of a=b=4.34 Å, and c=41.4 Å and the unit cell volume V=674.18 Å^3.[53-55] The c/a=9.55 of Bi_2GeTe_4 is much higher than that of Bi_2Te_3 (c/a=6.95), suggesting increased crystal complexity and a much lower κ_l.[46] In addition, Bi_2GeTe_4 has a relatively large Grüneisen parameter (γ=4.24) and a low average phonon velocity (V_{avg}=1540 m s^{-1}), which reflect high degree of anharmonicity and slow propagation of phonons, respectively.[52] Schroeder *et al.*[56] firstly reported that the zT of p-type Bi_2GeTe_4 is ~0.05 at room temperature. Singh *et al.*[52] found Bi_2GeTe_4 can be n-type with a peak zT of ~0.10 and a low $S^2\sigma$ of ~1.54 μW cm^{-1} K^{-2} at 350 K. Konstantinov *et al.*[57] further discovered that Bi_2GeTe_4 has a very close p-n transition point by minor adjustment of Ge content which suggests that the Fermi level (E_F) of Bi_2GeTe_4 should be close to the middle of the band gap. The n_c of Bi_2GeTe_4-based thermoelectric materials can change dramatically from 3.14×10^{19} cm^{-3} of p-type $Bi_2Ge_{0.98}Te_4$ to 2.06×10^{20} cm^{-3} of n-type $Bi_2Ge_{1.02}Te_4$ with tiny Ge content adjustment.[57,58] Meanwhile, p-type $Bi_2Ge_2Te_5$ (trigonal), with lattice parameters of a=b=4.3 Å, and c=17.36 Å, the unit cell volume V=278.13 Å^3 and the space group of *P3m1*,[59] can easily forms during the synthesis of Bi_2GeTe_4.[60] The phase content of $Bi_2Ge_2Te_5$ gradually increases with the increase of nominal Ge content (x of $Bi_2Ge_xTe_4$).[60] A key challenge for improving the thermoelectric performance of Bi_2GeTe_4-based thermoelectric materials is optimization of n_c.

To realize the optimization of n_c in Bi_2GeTe_4-based thermoelectric materials, we propose a stepwise strategy as shown in **Figure 1**a. Firstly, excessive Ge is introduced to reverse Ge deficiency, which can shift the E_F toward the conduction band as shown by the density function theory (DFT) calculation results in **Figure** 1b and c. The corresponding schematic crystal

structures are shown in **Figure S1**. Experimentally, it can transfer Bi_2GeTe_4-based materials into highly degenerated semiconductors. Secondly, additional p-type Ge vacancy-engineered $Bi_2Ge_2Te_5$ secondary phases (as shown in **Figure 1**d, where the E_F is deep in the valence band) are introduced to further tune the E_F toward the optimal level ($E_{F,opt}$) by further increasing the x. Overall, the proposed stepwise strategy can effective tune the position of E_F and the n_c, leading to high zT as schematically shown in **Figure 1**e. Correspondingly, comparing with previous works (**Figure 1**f), a high zT of ~0.22 and an optimized $S^2\sigma$ of ~4.2 μW cm^{-1} K^{-2} at 423 K are observed in $Bi_2Ge_{1.45}Te_4$ pellets prepared by a melting method in this study.

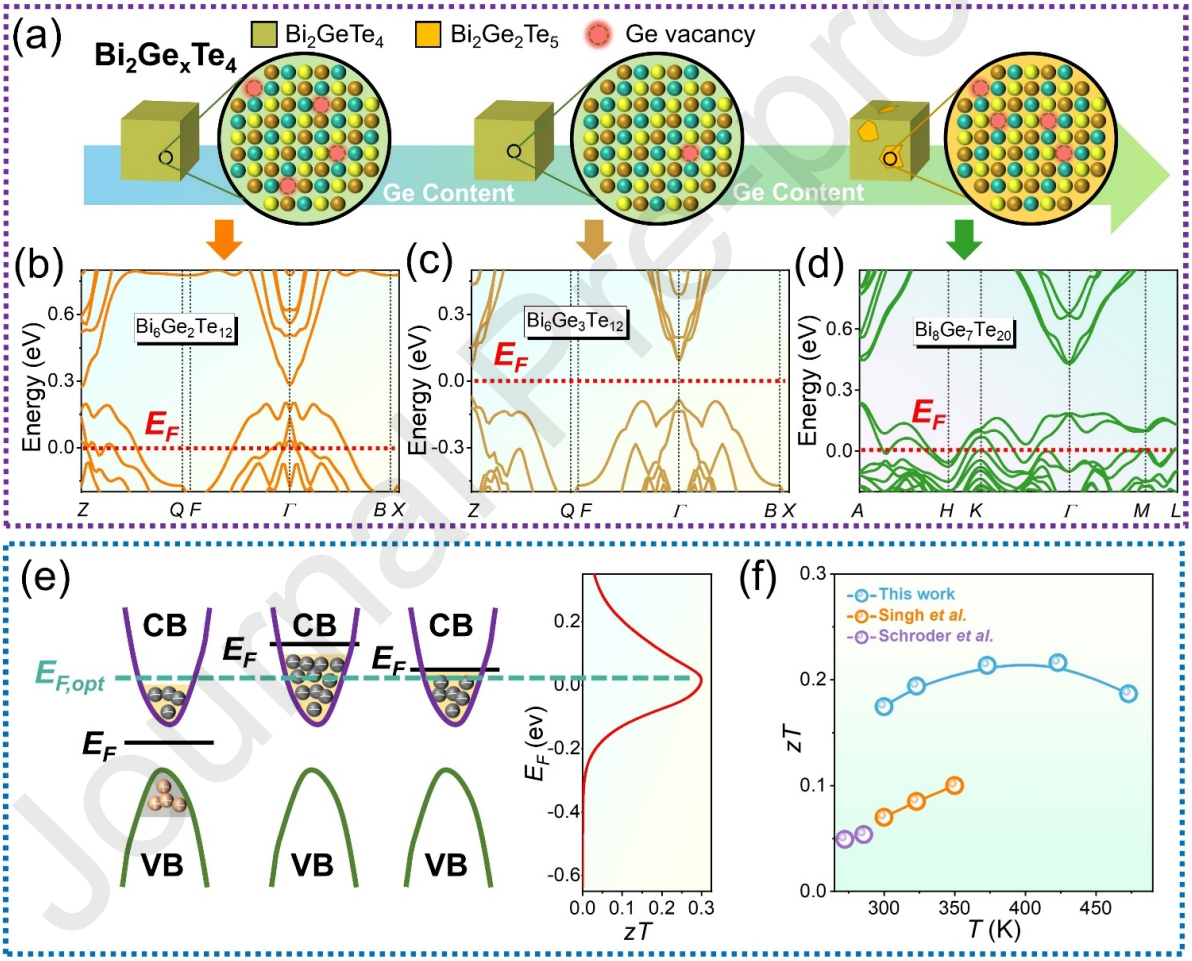

Figure 1.a) Schematic crystal structure and phase content change of as-synthesized $Bi_2Ge_xTe_4$ pellets with increasing x. b) DFT calculated band structures for vacancy-engineered Bi_2GeTe_4 ($Bi_6Ge_2Te_{12}$), c) pristine Bi_2GeTe_4 ($Bi_6Ge_3Te_{12}$) and d) Ge vacancy-engineered $Bi_2Ge_2Te_5$ ($Bi_8Ge_7Te_{20}$). e) Schematic change of E_F of as-sintered $Bi_2Ge_xTe_4$ pellets with increasing x and

single parabolic band (SPB) model-calculated the relationship between zT and E_F. f) Temperature-dependent zT of $Bi_2Ge_{1.45}Te_4$ in comparison with the experimental values of the Bi_2GeTe_4 pellets reported by Singh *et al*.[52] and Schroder *et al*.[56]

2. Experimental section

Material Synthesis: High purity Ge (99.99 %), Te (99.99 %) and Bi (99.99 %) precursors were purchased from China National Building Material (Chengdu) optoelectronic materials Co., Ltd. These precursors with the designed stoichiometric ratios of $Bi_2Ge_xTe_4$ (x=1-1.6) were sealed in quartz tubes under high vacuum (10^{-3} Pa), slowly heated to 1023 K in 12 h, dwelled for another 12 h and followed by quenching in ice water. The obtained ingots were ground into powder and vacuum-sintered by Spark Plasma Sintering (LABOX-110H Sinter Land) under the pressure of 55 MPa at 723 K for 5 min. The densities (ρ) of all sintered pellets were measured by the Archimedes method, where relative densities of all pellets are above 96 %.

Characterization: Powder X-ray diffraction (XRD, Smartlab 3 KW, with Cu source) was used to understand the crystal structure of as-prepared $Bi_2Ge_xTe_4$ pellets. Scanning Electron Microscope (SEM, Hitachi TM3000, Japan) equipped with Energy Dispersive X-ray Spectrometer (EDS) and Transmission Electron Microscopy (TEM, FEI Talos F200) were also used to investigate the crystal structures and chemical compositions. The EDS composition characterization error range is taken as ~5 wt. %, which is an integrated result based on both the composition difference at different spots/areas of the same sample and the equipment error range.

Thermoelectric Performance Measurement: σ and S were measured through the SBA 458 (NETZSCH, Germany) under an argon atmosphere. Room temperature S were measured by a portable device (PTM, JouleYacht, China). κ values were calculated based on $\kappa=D\times C_p\times\rho$, where D is the thermal diffusivity coefficient, C_p is the specific heat capacity. D values are

measured by a laser flash method (LFA 467, NETZSCH, Germany). C_p values were calculated by the Dulong-Petit law. The Hall coefficient (R_H) values were measured by the Van der Pauw method with a magnetic field up to ±1.5*T*. n_c and mobility (μ) were calculated using $n_c=1/(eR_H)$ and $\mu=\sigma R_H$, respectively, where *e* represents the electron charge.

Density Functional Theory Calculations: Band structure calculations were performed using Vienna Ab initio Simulation Package through a projector-augmented wave method. Generalized gradient approximation in form of fully relativistic Perdew-Burke-Ernzerhof functional was adopted to treat exchange correlation interactions. The supercells were constructed (*i.e.* 1×1×1 for Bi_2GeTe_4 and 2×2×1 for $Ge_2Bi_2Te_5$) to simulate the cases of Ge deficiency, with their Brillouin zones sampled by a 12×12×1 and 4×4×2 Monkhorst-Pack k-mesh grid, respectively. The density-of-state calculation was conducted on a mesh mode k-space with 1000 grid points dividing the energy spectrum, while the band structure calculation was conducted along a line-mode k-path (*e.g.* Z-Q-F-Γ-B-X) with Brillion paths feature from AFLOW framework. The spin-orbital coupling effect was considered for non-colinear calculations.

3. Results and discussion

Figure 2a shows the XRD patterns of the as-synthesized $Bi_2Ge_xTe_4$ (x=1-1.6) pellets. All pellets crystallize into the hexagonal Bi_2GeTe_4 (PDF#48-1340) when x≤1.2. When x>1.2, $Bi_2Ge_xTe_4$ (x=1.3-1.6) pellets contain both hexagonal Bi_2GeTe_4 and trigonal $Bi_2Ge_2Te_5$. With increasing x of $Bi_2Ge_xTe_4$, the intensities of Bi_2GeTe_4 XRD peaks reduce while those of $Bi_2Ge_2Te_5$ increase. To reveal the change of Bi_2GeTe_4 and $Bi_2Ge_2Te_5$ phases, we further plot peak intensity ratios between Bi_2GeTe_4 and all phases (Bi_2GeTe_4 and $Bi_2Ge_2Te_5$) in comparison with that between $Bi_2Ge_2Te_5$ and all phases in **Figure 2**b. As can be seen, when x≥1.3, $Bi_2Ge_2Te_5$ appears and $Bi_2Ge_2Te_5$ phase content increases sharply with increasing x. To

confirm the change of phase content in as-sintered $Bi_2Ge_xTe_4$ pellets, we performed corresponding EDS analyses. **Figure 2**c shows the back-scattered electron (BSE) images of the as-sintered Bi_2GeTe_4 (x=1) pellet with corresponding EDS maps. In as-sintered Bi_2GeTe_4 (x=1) pellet, no obvious impurities can be observed and Bi, Ge and Te are distributed homogeneously. When x=1.3, small amounts of dark areas can be observed in **Figure 2**d in accompany with the EDS spectra of both dark and bright areas. As can be seen, both dark and bright areas are composed of Bi, Ge and Te. Quantitative analyses suggest that the composition of the dark area is close to $Bi_2Ge_2Te_5$ while the bright area is close to Bi_2GeTe_4, which indicates the existence of two phases in the sample, consistent with the XRD results. With increasing the nominal x in $Bi_2Ge_xTe_4$ pellets, bright areas (Bi_2GeTe_4 phase) reduce and the dark areas ($Bi_2Ge_2Te_5$ phase) increase, as illustrated in **Figure S2** of the supporting information.

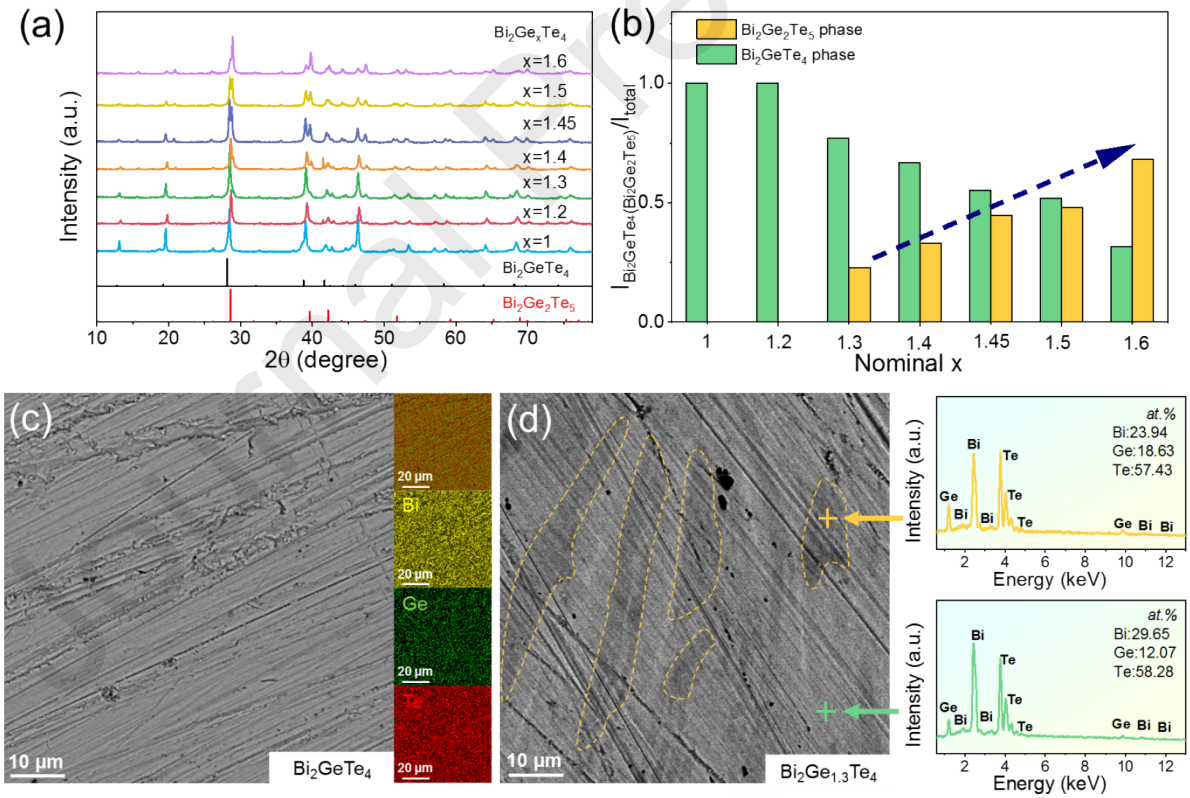

Figure 2. a) XRD patterns of as-sintered $Bi_2Ge_xTe_4$ (x=1-1.6) pellets. b) Peak intensity ratios between Bi_2GeTe_4 and all phases (Bi_2GeTe_4 and $Bi_2Ge_2Te_5$) in comparison with that between

$Bi_2Ge_2Te_5$ and all phases. c) BSE image and EDS maps of as-sintered Bi_2GeTe_4 pellet. d) BSE image of as-sintered $Bi_2Ge_{1.3}Te_4$ pellet and corresponding EDS spectra taken from the dark (upper right) and bright (lower right) areas.

To understand the compositional change of the Bi_2GeTe_4 main phase in the as-sintered $Bi_2Ge_xTe_4$ pellets, we performed corresponding EDS analyses as shown in **Figure 3**. **Figure 3**a, b and c show the BSE images of the as-sintered $Bi_2Ge_xTe_4$ pellets (x=1-1.6), corresponding typical EDS spectra and measured average Bi/Ge/Te stoichiometries of the bright areas (Bi_2GeTe_4 phase) in the form of $Bi_{2+h}Ge_{1+i}Te_4$ (h and i are the relative excess of Bi and Ge while assuming Te is assumed on stoichiometry), respectively. The measured 1+i of $Bi_2Ge_{1.2}Te_4$ pellet is higher than that of Bi_2GeTe_4 pellet, indicating that excess Ge suppresses the formation of Ge vacancies. And no obvious composition change can be observed as x of $Bi_2Ge_xTe_4$ increases from 1.2 to 1.45. With increasing the x from 1.45 to 1.6, additional Bi filling Ge vacancies can be observed in the Bi_2GeTe_4 phase.

Journal Pre-proofs

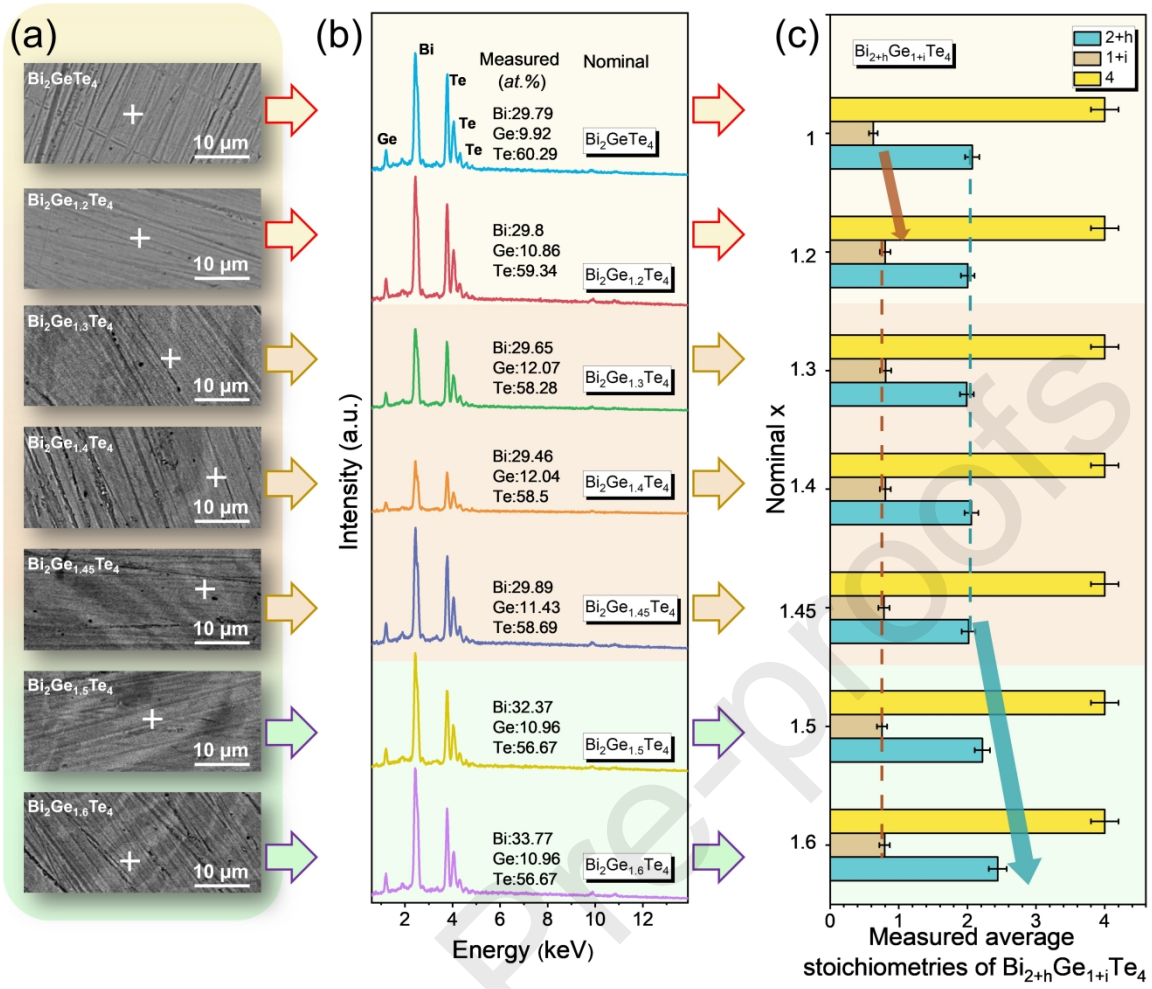

Figure 3. a) BSE images of as-sintered $Bi_2Ge_xTe_4$ (x=1-1.6) pellets. b) Typical EDS spectra taken from the bright areas (Bi_2GeTe_4 phase) as labelled in a). c) EDS measured average Bi/Ge/Te stoichiometries of the bright areas (Bi_2GeTe_4 phase) of as-sintered $Bi_2Ge_xTe_4$ (x=1-1.6) pellets in the form of $Bi_{2+h}Ge_{1+i}Te_4$.

To further characterize the composition and crystal structure of the as-formed $Bi_2Ge_2Te_5$ phase, EDS and TEM analyses were carried out. **Figure 4**a and b present measured average Bi/Ge/Te stoichiometries of $Bi_2Ge_2Te_5$ phase in the form of $Bi_{2+h}Ge_{2+i}Te_5$ (h and i are also the relative excess of Bi and Ge) of the dark areas ($Bi_2Ge_2Te_5$ phase) of as-sintered $Bi_2Ge_xTe_4$ (x=1.3-1.6) pellets and corresponding typical EDS spectra, respectively. As can be seen, all dark areas show similar compositions of $Bi_2Ge_{1.55}Te_5$ and no obvious difference can be

observed, which indicates the $Bi_2Ge_2Te_5$ phase contains a large amount of Ge vacancies. **Figure 4**c shows the typical TEM image of a lamella of dark areas of as-sintered $Bi_2Ge_{1.45}Te_4$ pellet prepared by microtome, where the inset is the enlarged image of the red-square-circled area. **Figure 4**d is the high-resolution TEM (HRTEM) image of the white-square-circled area in the inset of **Figure 4**c with the measured planar distances and angle consistent with the (010) and (005) planes of $Bi_2Ge_2Te_5$. Inset of **Figure 4**d is a reproduced image of the green-square-circled area of **Figure 4**d, where the lattice can well superimpose with the crystal structure of $Bi_2Ge_2Te_5$. This clearly evidences the existence of $Bi_2Ge_2Te_5$ in our $Bi_2Ge_{1.45}Te_4$ samples and indicates that the TEM characterization area should be the dark area of the BSE-SEM image of **Figure 2**d. Combining the XRD, SEM-EDS and TEM results, Bi_2GeTe_4 and $Bi_2Ge_2Te_5$ phases are the components of our $Bi_2Ge_xTe_4$ samples. The TEM sample should be cut-off from the dark areas. **Figure 4**e is the corresponding Fast Fourier Transform (FFT) pattern which can be indexed along the [100] of $Bi_2Ge_2Te_5$. **Figure 4**f shows the processed strain maps of the same area in **Figure 4d,** where dense strain fields can be observed, which should be attributed to the intrinsic Ge vacancies in as-formed $Bi_2Ge_2Te_5$ phase.

Journal Pre-proofs

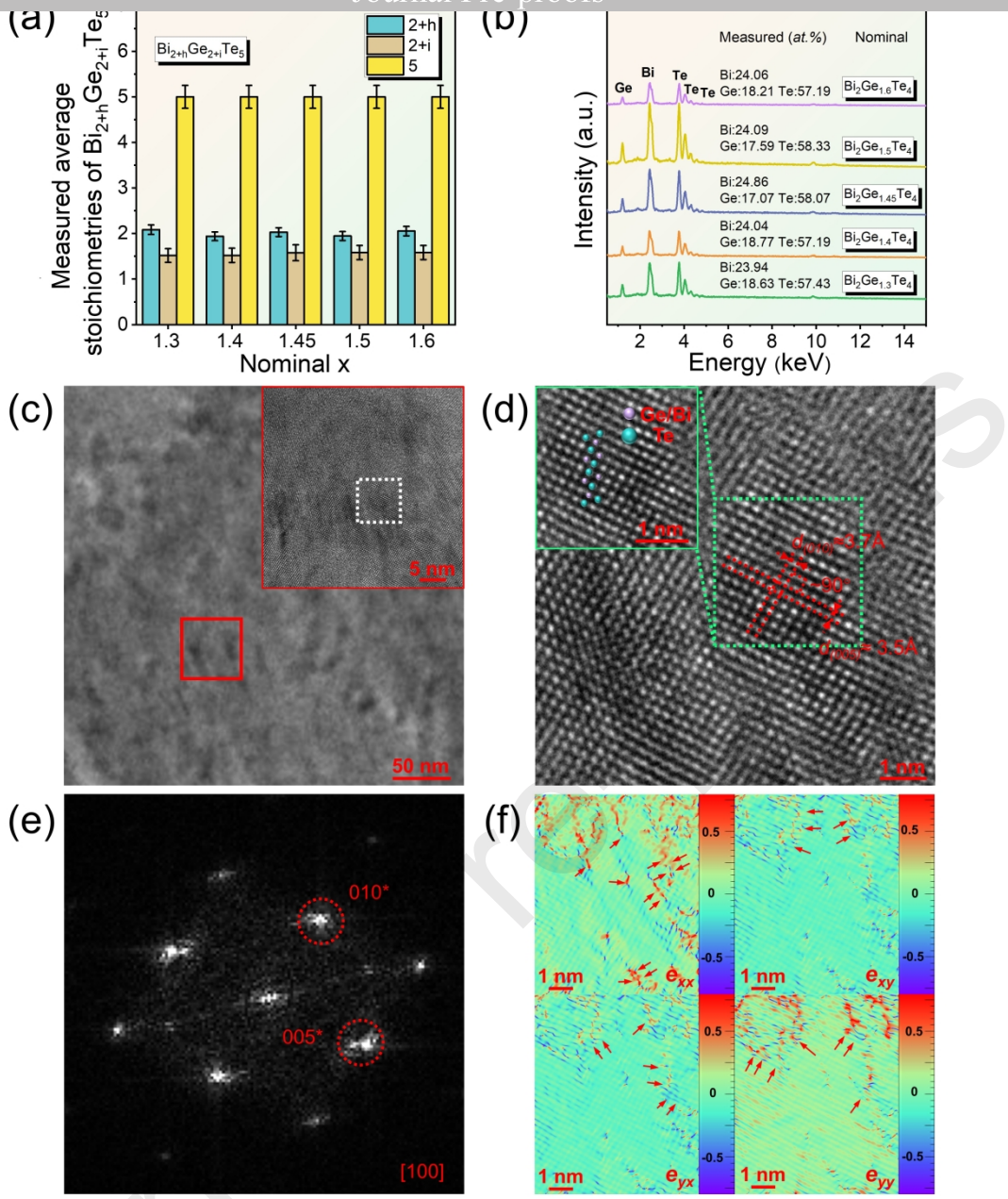

Figure 4. a) EDS measured average Bi/Ge/Te stoichiometries of $Bi_2Ge_2Te_5$ phase of as-sintered $Bi_2Ge_xTe_4$ (x=1.3-1.6) pellets in the form of $Bi_{2+h}Ge_{2+i}Te_5$. b) Typical EDS spectra of the dark areas ($Bi_2Ge_2Te_5$ phase) in $Bi_2Ge_xTe_4$ pellets (x=1.3-1.6). c) Low-magnification TEM image of a lamella in the dark areas of as-sintered $Bi_2Ge_{1.45}Te_4$ pellet prepared by microtome and inset is enlarged image of the red-square-circled area. d) HRTEM image of the white-square-circled area in the inset of c), inset is a reproduced image of the green-square-circled area. e) FFT pattern of d). f) Strain maps of the area same as d).

pellets measured at 423 K and corresponding temperature-dependent thermoelectric properties are shown in **Figure S3**. **Figure 5**a shows σ of the as-sintered $Bi_2Ge_xTe_4$ pellets as a function of nominal x. At 423 K, σ firstly increases with increasing the x from 1 to 1.2, and subsequently decreases from ~584 S cm^{-1} of $Bi_2Ge_{1.2}Te_4$ pellet to ~352 S cm^{-1} of $Bi_2Ge_{1.6}Te_4$ pellet. The reduced σ with increasing x from 1.2 to 1.6 should be dominated by dramatically reduced n_c as shown in **Figure 5**b. The n_e of $Bi_2Ge_xTe_4$ (x=1.2-1.6) samples is relatively high (10^{20}-10^{21} cm^{-3}), indicating that they are highly degenerate semiconductors. Additionally, the electrical performance of the as-prepared $Bi_2Ge_xTe_4$ samples did not change dramatically with increasing the temperature and no bipolar phenomenon has been observed in **Figure S3**a and b. Hence, we employed the room-temperature n_c for near-room temperature thermoelectric performance analyses. Corresponding, μ values are presented and discussed in **Figure S4** of the supporting information. **Figure 5**c schematically presents that with increasing the x from 1 to 1.2, excessive Ge firstly suppressed the formation of Ge vacancies and changed p-type Bi_2GeTe_4 into n-type $Bi_2Ge_{1.2}Te_4$. Further increasing the nominal x from 1.2 to 1.45, n_e dramatically decreases due to the increasing amount of p-type $Bi_2Ge_2Te_5$ phase.[61] With further increasing the nominal x of $Bi_2Ge_xTe_4$ from 1.45 to 1.6, Bi can fill out Ge vacancies and enhance n_e. **Figure 5**d shows the nominal x-dependent $|S|$ at 423 K. The $|S|$ at 423 K increases from 15 μV K^{-1} of the Bi_2GeTe_4 to 100 μV K^{-1} of the $Bi_2Ge_{1.45}Te_4$ due to both high material degeneration and decreased n_e. With increasing the nominal x of $Bi_2Ge_xTe_4$ from 1.45 to 1.6, The $|S|$ at 423 K decreases due to increased n_e. **Figure 5**e plots the n_e-dependent $S^2\sigma$ of as-sintered $Bi_2Ge_xTe_4$ (x=1.2-1.6) pellets in comparison with the SPB model calculated curves. Detailed calculations can be referred to Supporting Information. Dominated by the gradually optimized n_e, $S^2\sigma$ has been dramatically enhanced from 1.9 μW cm^{-1} K^{-2} of $Bi_2Ge_{1.2}Te_4$ pellet to 4.2 μW cm^{-1} K^{-2} of $Bi_2Ge_{1.45}Te_4$ pellet at 423 K. **Figure 5**f and g plots nominal x-dependent κ and κ_l of as-sintered $Bi_2Ge_xTe_4$ (x=1-1.6) pellets at 423 K. κ of as-sintered $Bi_2Ge_xTe_4$ is enhanced from ~0.71 W m^{-1} K^{-1} to ~0.87 W m^{-1} K^{-1} at 423 K with increasing the nominal x from 1 to 1.6. The change of κ is dominated by both κ_e (**Figure S5**) and κ_l. As can be seen, κ_l has

attributed to the increase of $Bi_2Ge_2Te_5$ phase whose κ_l is higher comparing with Bi_2GeTe_4.[61] **Figure 5**h plots E_F-dependent zT of as-sintered $Bi_2Ge_xTe_4$ (x=1.2-1.6) pellets with corresponding n_e in comparison with SPB model calculated E_F-dependent zT at 423 K. Detailed calculations of SPB model can be referred to Supporting Information. The E_F of $Bi_2Ge_{1.2}Te_4$ pellet is deep in the conduction band, leading to high n_e. With further increasing x, the E_F shifts close to the $E_{F,opt}$, leading to optimized n_e and significantly enhanced zT. The peak zT of as-sintered $Bi_2Ge_{1.45}Te_4$ pellet approaches up to 0.22 at 423 K. The optimal n_e of zT is different from that of the $S^2\sigma$, as the n_e-dependent κ_e needs to be considered for the zT, but excluded from the $S^2\sigma$.

Journal Pre-proofs

Journal Pre-proofs

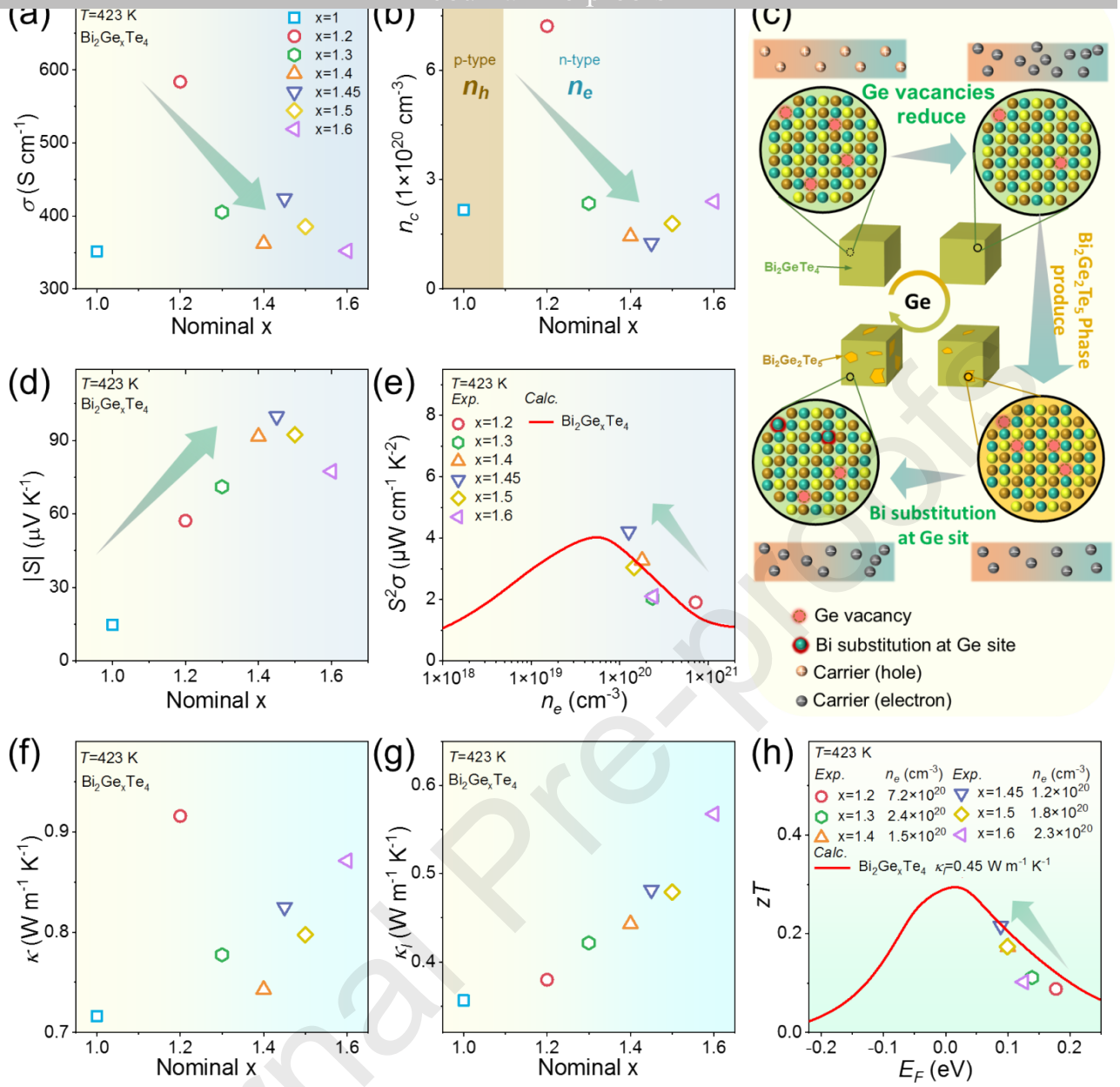

Figure. 5 a) Nominal x-dependent σ of as-sintered $Bi_2Ge_xTe_4$ (x=1-1.6) pellets at 423 K. b) Nominal x-dependent n_c of as-sintered $Bi_2Ge_xTe_4$ (x=1-1.6) pellets at room-temperature. c) Schematic diagram showing the microstructure and n_c change of as-sintered $Bi_2Ge_xTe_4$ (x=1-1.6) pellets with increasing x. d) Nominal x-dependent $|S|$ of as-sintered $Bi_2Ge_xTe_4$ (x=1-1.6) pellets at 423 K. e) SPB model calculated n_e-dependent $S^2\sigma$ at 423 K in comparison with the experimental values of $Bi_2Ge_xTe_4$ (x=1.2-1.6) pellets. f) Nominal x-dependent κ of as-sintered $Bi_2Ge_xTe_4$ (x=1-1.6) pellets at 423 K. g) Nominal x-dependent κ_l of as-sintered $Bi_2Ge_xTe_4$ (x=1-1.6) pellets at 423 K. h) SPB model calculated E_F-dependent zT at 423 K in comparison with the experimental values of $Bi_2Ge_xTe_4$ (x=1.2-1.6) pellets.

In this study, we propose an effective stepwise strategy to overcome the challenge of the n_e optimization in n-type Bi_2GeTe_4-based thermoelectric materials. Firstly, we introduce excessive Ge into Bi_2GeTe_4 to suppress the formation of Ge vacancies, which can correspondingly convert Bi_2GeTe_4 into highly degenerated n-type semiconductor by shifting the E_F deep into the conduction band. Secondly, the p-type $Bi_2Ge_2Te_5$ secondary phase is introduced through further increasing the Ge content, which can shift the E_F close to the optimal level and realize optimization of n_e. Consequently, optimized n_e leads to a high $S^2\sigma$ of 4.2 μW cm^{-1} K^{-2} at 423 K in as-sintered $Bi_2Ge_{1.45}Te_4$ pellet. A high zT of ~0.22 is obtained in the as-sintered n-type $Bi_2Ge_{1.45}Te_4$ pellet at 423 K. The zT of $Bi_2Ge_{1.45}Te_4$ pellet is 150 % higher than that of the currently reported Bi_2GeTe_4 pellet at the same temperature (300 K).[52]

Acknowledgements

Liang-cao Yin and Wei-Di Liu contributed equally to this work. This work was financially supported by the National Natural Science Foundation of China (No. 51972170), the State Key Laboratory of Materials-Oriented Chemical Engineering (No. ZK201812), the CAS Key Laboratory of Carbon Materials (No. KLCMKFJJ2002), the Priority Academic Program Development of Jiangsu Higher Education Institutions (PAPD), and the Jiangsu Specially-Appointed Professor Program. ZGC thanks the financial support from the Australian Research Council, and USQ strategic research grant.

Conflict of Interest

The authors declare no conflict of interest.

[1] G. Yang, L. Sang, F. F. Yun, D. R. G. Mitchell, G. Casillas, N. Ye, K. See, J. Pei, X. Wang, J.-F. Li, G. J. SnyderX. Wang, Significant Enhancement of Thermoelectric Figure of Merit in BiSbTe-Based Composites by Incorporating Carbon Microfiber, Adv. Funct. Mater. 31 (2021) 2008851.

[2] M. G. Voss, J. R. Challa, D. T. Scholes, P. Y. Yee, E. C. Wu, X. Liu, S. J. Park, O. Leon Ruiz, S. Subramaniyan, M. Chen, S. A. Jenekhe, X. Wang, S. H. TolbertB. J. Schwartz, Driving Force and Optical Signatures of Bipolaron Formation in Chemically Doped Conjugated Polymers, Adv. Mater. 33 (2021) 2000228.

[3] X.-L. Shi, J. ZouZ.-G. Chen, Advanced Thermoelectric Design: From Materials and Structures to Devices, Chem. Rev. 120 (2020) 7399-7515.

[4] S. Wang, Y. Xiao, Y. Chen, S. Peng, D. Wang, T. Hong, Z. Yang, Y. Sun, X. GaoL.-D. Zhao, Hierarchical Structures Lead to High Thermoelectric Performance in $Cu_{m+n}Pb_{100}Sb_mTe_{100}Se_{2m}$ (CLAST), Energy Environ. Sci. 14 (2021) 451-461.

[5] B. Jiang, Y. Yu, J. Cui, X. Liu, L. Xie, J. Liao, Q. Zhang, Y. Huang, S. Ning, B. Jia, B. Zhu, S. Bai, L. Chen, S. J. PennycookJ. He, High-Entropy-Stabilized Chalcogenides with High Thermoelectric Performance, Science 371 (2021) 830-834.

[6] W.-D. Liu, Y. Yu, M. Dargusch, Q. LiuZ.-G. Chen, Carbon Allotrope Hybrids Advance Thermoelectric Development and Applications, Renew. Sust. Energ. Rev 141 (2021) 110800.

[7] X.-L. Shi, H. Wu, Q. Liu, W. Zhou, S. Lu, Z. Shao, M. DarguschZ.-G. Chen, $SrTiO_3$-based Thermoelectrics: Progress and Challenges, Nano Energy 78 (2020) 105195.

[8] S. P. Zhan, L. Zheng, Y. XiaoL. D. Zhao, Phonon and Carrier Transport Properties in Low-Cost and Environmentally Friendly SnS_2: A Promising Thermoelectric Material, Chem. Mater. 32 (2020) 10348-10356.

[9] W.-D. Liu, Z.-G. ChenJ. Zou, Eco-Friendly Higher Manganese Silicide Thermoelectric Materials: Progress and Future Challenges, Adv. Energy Mater. 8 (2018) 1800056.

Wearable Electrocardiographic Systems, Adv. Sci. 7 (2020) 13.

[11] G. Yang, R. Niu, L. Sang, X. Liao, D. R. G. Mitchell, N. Ye, J. Pei, J.-F. LiX. Wang, Ultra-High Thermoelectric Performance in Bulk BiSbTe/Amorphous Boron Composites with Nano-Defect Architectures, Adv. Energy Mater. 10 (2020) 2000757.

[12] W. D. Liu, L. YangZ. G. Chen, Cu_2Se Thermoelectrics: Property, Methodology, and Device, Nano Today 35 (2020) 24.

[13] Y. Wang, M. Hong, W. D. Liu, X. L. Shi, S. D. Xu, Q. Sun, H. Gao, S. Y. Lu, J. ZouZ. G. Chen, $Bi_{0.5}Sb_{1.5}Te_3$/PEDOT:PSS-based Flexible Thermoelectric Film and Device, Chem. Eng. J. 397 (2020) 9.

[14] Z. Zhang, K. Zhao, T.-R. Wei, P. Qiu, L. ChenX. Shi, Cu_2Se-Based Liquid-like Thermoelectric Materials: Looking Back and Stepping Forward, Energy Environ. Sci. 13 (2020) 3307-3329.

[15] W. D. Liu, X. L. Shi, R. Moshwan, L. Yan, Z. G. ChenJ. Zou, Solvothermal Synthesis of High-purity Porous $Cu_{1.7}Se$ Approaching Low Lattice Thermal Conductivity, Chem. Eng. J. 375 (2019) 7.

[16] Y. Pei, X. Shi, A. LaLonde, H. Wang, L. ChenG. J. Snyder, Convergence of Electronic Bands for High Performance Bulk Thermoelectrics, Nature 473 (2011) 66-69.

[17] Z. Bu, X. Zhang, B. Shan, J. Tang, H. Liu, Z. Chen, S. Lin, W. LiY. Pei, Realizing a 14% Single-leg Thermoelectric Efficiency in GeTe Alloys, Sci. Adv. 7 (2021) eabf2738.

[18] X. Zhang, J. Li, X. Wang, Z. Chen, J. Mao, Y. ChenY. Pei, Vacancy Manipulation for Thermoelectric Enhancements in GeTe Alloys, J. Am. Chem. Soc. 140 (2018) 15883-15888.

[19] Q. Sun, M. Li, X.-L. Shi, S.-D. Xu, W.-D. Liu, M. Hong, W.-y. Lyu, Y. Yin, M. Dargusch, J. ZouZ.-G. Chen, Versatile Vanadium Doping Induces High Thermoelectric Performance in GeTe via Band Alignment and Structural Modulation, Adv. Energy Mater. 11 (2021) 2100544.

Y. Liu, L. Miao, D. Nan, T. M. WangL. D. Zhao, Record High Thermoelectric Performance in Bulk $SrTiO_3$ Via Nano-scale Modulation Doping, Nano Energy 35 (2017) 387-395.

[21] Y.-L. Pei, H. Wu, D. Wu, F. ZhengJ. He, High Thermoelectric Performance Realized in a BiCuSeO System by Improving Carrier Mobility through 3D Modulation Doping, J. Am. Chem. Soc. 136 (2014) 13902-13908.

[22] T. Xing, C. X. Zhu, Q. F. Song, H. Huang, J. Xiao, D. D. Ren, M. J. Shi, P. F. Qiu, X. Shi, F. F. XuL. D. Chen, Ultralow Lattice Thermal Conductivity and Superhigh Thermoelectric Figure-of-Merit in (Mg, Bi) Co-Doped GeTe, Adv. Mater. 33 (2021) 9.

[23] D. Yang, X. Su, Y. Yan, T. Hu, H. Xie, J. He, C. Uher, M. G. KanatzidisX. Tang, Manipulating the Combustion Wave during Self-Propagating Synthesis for High Thermoelectric Performance of Layered Oxychalcogenide $Bi_{1-x}Pb_xCuSeO$, Chem. Mater. 28 (2016) 4628-4640.

[24] P. PichanusakornP. Bandaru, Nanostructured thermoelectrics, Mat. Sci. Eng. R. 67 (2010) 19-63.

[25] M. Samanta, T. Ghosh, S. ChandraK. Biswas, Layered Materials with 2D Connectivity for Thermoelectric Energy Conversion, J. Mater. Chem. A 8 (2020) 12226-12261.

[26] Y. Zhang, B. Feng, H. Hayashi, C.-P. Chang, Y.-M. Sheu, I. Tanaka, Y. IkuharaH. Ohta, Double Thermoelectric Power Factor of a 2D Electron System, Nat. Commun. 9 (2018) 2224.

[27] Y. Zhao, P. Yu, G. Zhang, M. Sun, D. Chi, K. Hippalgaonkar, J. T. L. ThongJ. Wu, Low-Symmetry $PdSe_2$ for High Performance Thermoelectric Applications, Adv. Funct. Mater. 30 (2020) 2004896.

[28] M. Hong, Y. Wang, W. Liu, S. Matsumura, H. Wang, J. ZouZ.-G. Chen, Arrays of Planar Vacancies in Superior Thermoelectric $Ge_{1-x-y}Cd_xBi_yTe$ with Band Convergence, Adv. Energy Mater. 8 (2018) 1801837.

Chen, Crystal Symmetry Induced Structure and Bonding Manipulation Boosting Thermoelectric Performance of GeTe, Nano Energy 73 (2020) 104740.

[30] R. Moshwan, W.-D. Liu, X.-L. Shi, Y.-P. Wang, J. ZouZ.-G. Chen, Realizing High Thermoelectric Properties of SnTe Via Synergistic Band Engineering and Structure Engineering, Nano Energy 65 (2019) 104056.

[31] F. Qin, S. A. Nikolaev, A. Suwardi, M. Wood, Y. Zhu, X. Tan, U. Aydemir, Y. Ren, Q. Yan, L. HuG. J. Snyder, Crystal Structure and Atomic Vacancy Optimized Thermoelectric Properties in Gadolinium Selenides, Chem. Mater. 32 (2020) 10130-10139.

[32] W.-D. Liu, D.-Z. Wang, Q. Liu, W. Zhou, Z. ShaoZ.-G. Chen, High-Performance GeTe-Based Thermoelectrics: from Materials to Devices, Adv. Energy Mater. 10 (2020).

[33] M. Hong, Z. G. Chen, L. Yang, Y. C. Zou, M. S. Dargusch, H. WangJ. Zou, Realizing zT of 2.3 in $Ge_{1-x-y}Sb_xIn_yTe$ via Reducing the Phase-Transition Temperature and Introducing Resonant Energy Doping, Adv. Mater. 30 (2018) 1705942.

[34] J. F. Dong, C. F. Wu, J. Pei, F. H. Sun, Y. Pan, B. P. Zhang, H. C. TangJ. F. Li, Lead-free MnTe Mid-temperature Thermoelectric Materials: Facile Synthesis, p-Type Doping and Transport Properties, J. Mater. Chem. C 6 (2018) 4265-4272.

[35] Z. H. Hou, D. Y. Wang, T. Hong, Y. X. Qin, S. Peng, G. T. Wang, J. F. Wang, X. Gao, Z. W. HuangL. D. Zhao, Boosting Thermoelectric Performance of n-Type PbS through Synergistically Integrating In Resonant Level and Cu Dynamic Doping, J. Phys. Chem. Solids 148 (2021) 10.

[36] M. Hong, Y. Wang, T. Feng, Q. Sun, S. Xu, S. Matsumura, S. T. Pantelides, J. ZouZ.-G. Chen, Strong Phonon-Phonon Interactions Securing Extraordinary Thermoelectric $Ge_{1-x}Sb_xTe$ with Zn-Alloying-Induced Band Alignment, J. Am. Chem. Soc. 141 (2019) 1742-1748.

Thermoelectric Performance of $AgSb_{1-x}Pb_xSe_2$ Prepared by Fast Nonequilibrium Synthesis, ACS Appl. Mater. Interfaces 12 (2020) 41333-41341.

[38] M. Li, D. L. Cortie, J. Liu, D. Yu, S. M. K. N. Islam, L. Zhao, D. R. G. Mitchell, R. A. Mole, M. B. Cortie, S. DouX. Wang, Ultra-high Thermoelectric Performance in Graphene Incorporated Cu_2Se: Role of Mismatching Phonon Modes, Nano Energy 53 (2018) 993-1002.

[39] V. Karthikeyan, C. M. Arava, M. Z. Hlaing, B. Chen, C. H. Chan, K.-H. LamV. A. L. Roy, Dislocation-induced Ultra-low Lattice Thermal Conductivity in Rare Earth Doped Beta-Zn_4Sb_3, Scripta Mater. 174 (2020) 95-101.

[40] L.-C. Yin, W.-D. Liu, M. Li, Q. Sun, H. Gao, D.-Z. Wang, H. Wu, Y.-F. Wang, X.-L. Shi, Q. LiuZ.-G. Chen, High Carrier Mobility and High Figure of Merit in the $CuBiSe_2$ Alloyed GeTe, Adv. Energy Mater. (2021) DOI: https://doi.org/10.1002/aenm.202102913

[41] Y.-X. Chen, Z.-H. Ge, M. Yin, D. Feng, X.-Q. Huang, W. ZhaoJ. He, Understanding of the Extremely Low Thermal Conductivity in High-Performance Polycrystalline SnSe through Potassium Doping, Adv. Funct. Mater. 26 (2016) 6836-6845.

[42] Q. Zhang, Z. Zhou, M. Dylla, M. T. Agne, Y. Pei, L. Wang, Y. Tang, J. Liao, J. Li, S. Bai, W. Jiang, L. ChenG. J. Snyder, Realizing High-performance Thermoelectric Power Generation through Grain Boundary Engineering of Skutterudite-based Nanocomposites, Nano Energy 41 (2017) 501-510.

[43] L. Hu, Y. Luo, Y.-W. Fang, F. Qin, X. Cao, H. Xie, J. Liu, J. Dong, A. Sanson, M. Giarola, X. Tan, Y. Zheng, A. Suwardi, Y. Huang, K. Hippalgaonkar, J. He, W. Zhang, J. Xu, Q. YanM. G. Kanatzidis, High Thermoelectric Performance through Crystal Symmetry Enhancement in Triply Doped Diamondoid Compound Cu2SnSe3, Adv. Energy Mater. n/a (2021) 2100661.

[44] C. Wan, Y. Wang, W. Norimatsu, M. KusunokiK. Koumoto, Nanoscale Stacking Faults Induced Low Thermal Conductivity in Thermoelectric Layered Metal Sulfides, Appl. Phys. Lett. 100 (2012) 101913.

Medium-temperature thermoelectric GeTe: vacancy suppression and band structure engineering leading to high performance, Energy Environ. Sci. 12 (2019) 1396-1403.

[46] N. K. Singh, J. Pandey, S. AcharyaA. Soni, Charge Carriers Modulation and Thermoelectric Performance of Intrinsically p-Type Bi_2Te_3 by Ge Doping, J. Alloys Compd. 746 (2018) 350-355.

[47] W. Wei, C. Chang, T. Yang, J. Z. Liu, H. C. Tang, J. Zhang, Y. S. Li, F. Xu, Z. D. Zhang, J. F. LiG. D. Tang, Achieving High Thermoelectric Figure of Merit in Polycrystalline SnSe via Introducing Sn Vacancies, J. Am. Chem. Soc. 140 (2018) 499-505.

[48] Y. Gan, Y. Huang, N. Miao, J. ZhouZ. Sun, Novel IV-V-VI semiconductors with ultralow lattice thermal conductivity, J. Mater. Chem. C 9 (2021) 4189-4199.

[49] F. Cai, R. Dong, W. Sun, X. Lei, B. Yu, J. Chen, L. Yuan, C. WangQ. Zhang, PbmBi2S3+m Homologous Series with Low Thermal Conductivity Prepared by the Solution-Based Method as Promising Thermoelectric Materials, Chem. Mater. 33 (2021) 6003-6011.

[50] M. Xi, H. Zhu, H. Wu, Y. Yang, Y. Yan, G. Wang, G. Wang, J. Li, X. LuX. Zhou, Thermoelectricity of n-type MnBi4S7-7xSe7x solid solution, Chem. Eng. J. 396 (2020) 125219.

[51] L. Hu, Y.-W. Fang, F. Qin, X. Cao, X. Zhao, Y. Luo, D. V. M. Repaka, W. Luo, A. Suwardi, T. Soldi, U. Aydemir, Y. Huang, Z. Liu, K. Hippalgaonkar, G. J. Snyder, J. XuQ. Yan, High thermoelectric performance enabled by convergence of nested conduction bands in Pb7Bi4Se13 with low thermal conductivity, Nat. Commun. 12 (2021) 4793.

[52] N. K. SinghA. Soni, Crystalline Anharmonicity and Ultralow Thermal Conductivity in Layered Bi_2GeTe_4 for Thermoelectric Applications, Appl. Phys. Lett. 117 (2020) 123901.

[53] R. Peng, Y. Ma, H. Wang, B. HuangY. Dai, Stacking-dependent Topological Phase in Bilayer MBi_2Te_4(M=Ge,Sn,Pb), Phys. Rev. B 101 (2020) 115427.

Crystal Structures and Thermoelectric Properties of Layered Compounds in the ATe-Bi_2Te_3 (A = Ge, Sn, Pb) Systems, Inorg. Mater+. 40 (2004) 451-460.

[55] O. G. Karpinsky, L. E. Shelimova, M. A. KretovaJ. P. Fleurial, X-ray Study of the nGeTe · mBi_2Te_3 Mixed Layered Tetradymite-like Compounds, J. Alloys Compd. 265 (1998) 170-175.

[56] T. Schroder, M. N. Schneider, T. Rosenthal, A. Eisele, C. Gold, E. W. Scheidt, W. Scherer, R. BertholdO. Oeckler, Nanostructures in Metastable $GeBi_2Te_4$ Obtained by High-pressure Synthesis and Rapid Quenching and their Influence on Physical Properties, Phys. Rev. B 84 (2011) 10.

[57] P. P. Konstantinov, L. E. Shelimova, E. S. Avilov, M. A. KretovaJ. P. Fleurial, Transport Phenomena in Mixed Layered Tetradymite-like Compounds in the GeTe-Bi_2Te_3 System, J. Solid State Chem. 146 (1999) 305-312.

[58] O. G. Karpinskii, L. E. Shelimova, M. A. KretovaE. C. Avilov, X-ray Study and Electrical Properties of the Layered $Ge_{1\pm\delta}Bi_2Te_4$ Semiconducting Compound, Physica Status Solidi (a) 142 (1994) 307-314.

[59] T. Matsunaga, R. Kojima, N. Yamada, K. Kifune, Y. KubotaM. Takata, Structures of Stable and Metastable $Ge_2Bi_2Te_5$, an Intermetallic Compound in a GeTe-Bi_2Te_3 Pseudobinary System, Acta Crystallogr. B 63 (2007) 346-352.

[60] L. E. Shelimova, O. G. Karpinsky, M. A. KretovaE. S. Avilov, Phase Equilibria in the Ge-Bi-Te Ternary System at 570-770 K Temperature Range, J. Alloys Compd. 243 (1996) 194-201.

[61] L. E. Shelimova, P. P. Konstantinov, O. G. Karpinsky, E. S. Avilov, M. A. KretovaV. S. Zemskov, X-Ray Diffraction Study and Electrical and Thermal Transport Properties of the nGeTe·mBi_2Te_3 Homologous Series Compounds, J. Alloys Compd. 329 (2001) 50-62.

- Stepwise carrier concentration optimization of Bi_2GeTe_4 thermoelectric materials.
- Ge vacancy-engineering transfer Bi_2GeTe_4 into highly degenerated semiconductor.
- Carrier concentration optimization leads to high power factor of 4.2 μW cm^{-1} K^{-2}.

Journal Pre-proofs